# Relativistic electronic structure, effective masses, and inversion-asymmetry effects of cubic silicon carbide (3C-SiC)

M. Willatzen and M. Cardona
*Max-Planck-Institut für Festkörperforschung, Heisenbergstrasse 1, D-70569 Stuttgart, Federal Republic Germany*

N. E. Christensen
*Institute of Physics and Astronomy, University of Aarhus, DK-8000 Aarhus C, Denmark*
(Received 26 September 1994; revised manuscript received 17 January 1995)

We present relativistic linear muffin-tin-orbital calculations of the electronic structure of zinc-blende-type silicon carbide (3C-SiC) within the local-density approximation. Information about matrix elements, effective masses, Luttinger parameters, as well as linear and cubic spin splittings due to inversion-asymmetry effects is extracted by comparison with $\vec{k}\cdot\vec{p}$ calculations. Ionicity and transverse effective charge are also discussed. The parameters determined in this way are subsequently used as input in an extended $16\times16$ $\vec{k}\cdot\vec{p}$ calculation so as to obtain the detailed band structure of the higher valence and the lower conduction band states around the $\Gamma$ point in the [100], [110], and [111] directions.

## I. INTRODUCTION

Silicon carbide has the potential to become an important candidate for high-temperature semiconductor devices. The material [together with semiconducting diamond (C) and boron nitride (BN)] is characterized by a number of interesting properties: a high melting point, high thermal conductivity, large band gap, high hardness, and chemical inertness.[1,2] However, experimental work on SiC has long been hindered by the difficulty of obtaining homogeneous single crystals, which is due in part to the large number (more than a 100) of different crystal modifications or polytypes.[1,6–10,23] The cubic modification (3C-SiC), which will be discussed here, is the only IV-IV compound with zinc-blende structure that exists in nature and therefore is an intermediate between III-V semiconductors and crystals with the diamond structure. In the past decade, large epitaxial 3C-SiC films have been grown on carbonized Si surfaces by the chemical vapor deposition technique.[3,4] In this way, both $n$- and $p$-type SiC have been obtained by introducing active impurities in the crystals. In spite of the considerable experimental and theoretical work performed over the past 40 years, very little is known about band parameters and effective masses of 3C-SiC. To the authors knowledge, only one set of Luttinger parameters has been reported to date,[5] and few results for the effective masses at the conduction band minimum located very close to the zone boundary $X$ have been published.[1,6]

In the present work, we use relativistic (with the spin-orbit interaction treated as a perturbation) linear muffin-tin-orbital (LMTO) band structure calculations in the local-density approximation assisted by $\vec{k}\cdot\vec{p}$ calculations to obtain information about momentum matrix elements, effective masses, Luttinger parameters, spin-orbit energies, cubic and linear spin-splitting coefficients, ionicity, and transverse effective charge of zinc-blende-type SiC. The parameters found are subsequently used as input in a $16\times16$ $\vec{k}\cdot\vec{p}$ model[11] involving matrix elements between six $\Gamma_{15}^{v}$, six $\Gamma_{15}^{c}$, two $\Gamma_{1}^{c}$, and two $\Gamma_{1}^{\prime c}$ wave functions. In this way, the detailed upper valence and the lower conduction band structure around the $\Gamma$ point is determined. Results in the [100], [110], and [111] directions are presented. The analysis of the calculated band splittings linear in $\vec{k}$ sheds considerable light on the responsible intermediate states and the systematics of these splittings in other zinc-blende-type materials.

## II. LMTO BAND STRUCTURE CALCULATIONS

We have calculated the electronic band structure of zinc-blende-type SiC (3C-SiC) within the framework of density-functional theory using the local-density approximation (LDA). Since we are interested in investigating inversion-asymmetry-induced spin splittings in SiC due to spin-orbit interaction, we treat the spin-orbit contribution as a perturbation to the Hamiltonian by means of the self-consistent LMTO method.[12] Each unit cell consists of four "atoms" including two "empty spheres," i.e., atomic spheres with no net nuclear charge positioned in the empty tetrahedral sites in order to obtain a close-packed structure.[13] Wave functions in all four "atomic spheres" are expressed in terms of $s$, $p$, and $d$ partial waves resulting in a Hamiltonian matrix of dimension 72 $\times$ 72 (4 atoms $\times$ 9 partial waves $\times$ 2 spin states). Calculations are performed in the usual way within the atomic-sphere approximation including the so-called combined correction term.[14]

The energy gaps across the Fermi level calculated within LDA are underestimated as a consequence of the fact that LDA energy values are not exact single-particle energies (the so-called gap problem). A way to overcome this problem is given by the $GW$ approxima-

 ©1995 The American Physical Society

tion,[15,16] where quasiparticle corrections are treated perturbatively. Even though the conduction band energies are underestimated in LDA, wave functions are essentially unchanged by self-energy contributions in the $GW$ approach. This trend follows for materials ranging from wide to narrow gap as well as from covalent to ionic bonding. As a result we expect momentum matrix elements, determined solely by the wave functions, to be well described by the LMTO calculations.

We use this information in the present paper in order to determine effective masses and Luttinger parameters of $3C$-SiC by using the LMTO LDA calculated momentum matrix elements as input in $\vec{k}\cdot\vec{p}$ models. Correcting for the discrepancy between the experimental and the calculated energy gaps, we expect the effective masses calculated in this way to be quite accurate since momentum matrix elements from the LMTO calculation are supposed to be accurate.[17] Transverse and longitudinal effective masses at the lowest conduction band minimum (our results show that this minimum is indeed located at the $X$ point) are also determined. Using as input the calculated matrix elements, Luttinger parameters, spin-orbit energies, and energy gaps in an extended $16\times 16$ $\vec{k}\cdot\vec{p}$ calculation[11] we determine the detailed upper valence and the lower conduction band structure of zinc-blende-type SiC at the $\Gamma$ point in the [100], [110], and [111] directions.

In order to ensure a consistent definition of the sign of the spin-orbit parameter $\Delta^-$, representing the coupling between the $\Gamma^c_{15}$ conduction and the $\Gamma^v_{15}$ valence bands, and the matrix elements $P$, $P'$, $Q$, and $P'''$ defined as[11]

$$P = i\langle\Gamma^v_{15,x} \mid p_x \mid \Gamma^c_1\rangle,\quad P' = i\langle\Gamma^c_{15,x} \mid p_x \mid \Gamma^c_1\rangle\ ,$$
$$Q = i\langle\Gamma^v_{15,x} \mid p_y \mid \Gamma^c_{15,z}\rangle,\quad P''' = i\langle\Gamma^c_{15,x} \mid p_x \mid \Gamma'^c_1\rangle\ , \tag{1}$$

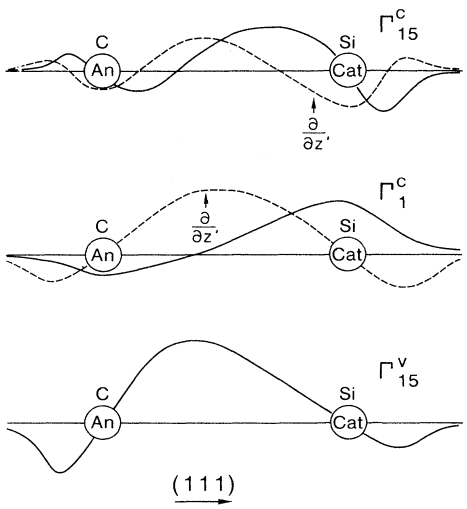


FIG. 1. Schematic diagram demonstrating the phase convention of the $\Gamma^c_{15}$, $\Gamma^v_{15}$, and $\Gamma^c_1$ wave functions. The C atom is taken to lie at the origin and corresponds to the anion (An). The cation (Si) is labeled (Cat). In the figure, the $z'$ direction corresponds to [111].

the positions chosen for the two constituent atoms must be specified and also the phase of the wave functions at $\Gamma$, which are conveniently chosen to be real (possible because of time-reversal symmetry), as depicted in Fig. 1. The C atom has been chosen to be at the origin, while Si is located at $a_0(\frac{1}{4},\frac{1}{4},\frac{1}{4})$, where $a_0$ is the lattice constant. This choice results in a positive sign for $P$ and $Q$, which is evident from Fig. 1 by replacing $p_x = -i\frac{\partial}{\partial x}$ (in atomic units, $\hbar = m_0 = e = 1$).

## III. EFFECTIVE MASSES AND MATRIX ELEMENTS

Spin-orbit effects are very small in $3C$-SiC.[5] The parameters $L$, $M$, $N$, and $A'$ introduced by Dresselhaus *et al.*[18] and Kane[19] and appearing in the expressions for effective masses are therefore well described by LMTO calculations without the inclusion of spin-orbit effects. $\vec{k}\cdot\vec{p}$ expressions for the effective masses at the $\Gamma$ point are given by Kane[19] and Shtivel'man[20] for the case of zero spin-orbit interactions ($\Delta_0 = 0$):

$$m_1^{-1} = 1 + 2L\ ,$$
$$m_2^{-1} = m_3^{-1} = 1 + 2M \tag{2}$$

in the [100] direction,

$$m_1^{-1} = 1 + \frac{2L + 4M + 4N}{3}\ ,$$
$$m_2^{-1} = m_3^{-1} = 1 + \frac{4M + 2L - 2N}{3} \tag{3}$$

in the [111] direction, and

$$m_1^{-1} = 1 + L + M + N\ ,$$
$$m_2^{-1} = 1 + 2M + \frac{1}{2}(L - M - N) - \frac{1}{2} \mid L - M - N \mid\ ,$$
$$m_3^{-1} = 1 + 2M + \frac{1}{2}(L - M - N) + \frac{1}{2} \mid L - M - N \mid \tag{4}$$

in the [110] direction. Here the subscripts of the effective masses increase with energy. The $s$-type conduction band ($\Gamma^c_1$) effective mass $m_4$ is isotropic and given by

$$m_4^{-1} = 1 + 2A' + \frac{2P^2}{E_0}\ , \tag{5}$$

where $E_0 = E_{\Gamma^c_6} - E_{\Gamma^v_8}$. The physically more meaningful hole masses $m_{\rm hh}$, $m_{\rm lh}$, and $m_{\rm so}$ and the conduction band mass $m_c$ including the spin-orbit splitting at $\Gamma$ are[19]

$$m_{\rm lh}^{-1} = 1 + \frac{2L + 4M - 2 \mid L - M \mid}{3},$$
$$m_{\rm hh}^{-1} = 1 + \frac{2L + 4M + 2 \mid L - M \mid}{3} \tag{6}$$

in the [100] direction,

$$m_{\rm lh}^{-1} = 1 + \frac{2L + 4M - 2 \mid N \mid}{3} ,$$
$$m_{hh}^{-1} = 1 + \frac{2L + 4M + 2 \mid N \mid}{3} \qquad (7)$$

in the [111] direction,

$$m_{\rm lh}^{-1} = 1 + \frac{2L + 4M - \left[(L-M)^2 + 3N^2\right]^{1/2}}{3},$$
$$m_{\rm hh}^{-1} = 1 + \frac{2L + 4M + \left[(L-M)^2 + 3N^2\right]^{1/2}}{3}, \qquad (8)$$

in the [110] direction, and

$$m_{\rm so}^{-1} = 1 + 2\left(\frac{2G + 2M}{3} - \frac{P^2}{3(E_0 + \Delta_0)}\right) ,$$
$$m_c^{-1} = 1 + 2A' + \frac{2P^2}{3}\left(\frac{2}{E_0} + \frac{1}{E_0 + \Delta_0}\right) \qquad (9)$$

for an isotropic effective mass. Note that the effective mass $m_c$ refers to the $s$-type conduction band, which is located below the $p$-type conduction band; see Fig. 2. This is in agreement with $GW$ calculations[16] and previous LMTO calculations[21,22] on cubic silicon carbide and opposite the case of diamond (C) and silicon. In diamond, the $\Gamma_1^c$ state is located 10.52 eV (LMTO LDA) (Ref. 17) and 8.0 ± 0.5 eV (experiment) (Ref. 23) above the $\Gamma_{15}^c$ states. In our discussion of effective masses, we use atomic units, i.e., $m_0 = \hbar = e = 1$, energies in hartree units, and Luttinger parameters in the conventional units of $\frac{\hbar^2}{2m_0}$.

The parameters $L$, $M$, $N$, and $A'$ are given by Dresselhaus *et al.*[18] and Kane:[19]

$$L = F + 2G ,$$
$$M = H_1 + H_2 ,$$
$$N = F - G + H_1 - H_2 , \qquad (10)$$

where

$$F \approx -\frac{P^2}{E_{\Gamma_1^c} - E_{\Gamma_{15}^v}} ,$$
$$G \approx -\frac{R^2}{E_{\Gamma_{12}} - E_{\Gamma_{15}^v}} ,$$
$$H_1 \approx -\frac{Q^2}{E_{\Gamma_{15}^c} - E_{\Gamma_{15}^v}} ,$$
$$H_2 \approx 0 ,$$
$$A' \approx \frac{P'^2}{E_{\Gamma_1^c} - E_{\Gamma_{15}^c}} + \frac{S^2}{E_{\Gamma_1^c} - E_{\Gamma_{15}^{\prime c}}} , \qquad (11)$$

and

$$R = i\langle \Gamma_{15,x}^v \mid p_x \mid \Gamma_{12,1} \rangle ,$$
$$S = i\langle \Gamma_{15,x}^{\prime c} \mid p_x \mid \Gamma_1^c \rangle . \qquad (12)$$

The matrix elements $P$, $P'$, and $Q$ above were defined in Eq. (1). The $\Gamma_{12,1}$ state in Eq. (12) is equivalent to the $\gamma_1^-$-state of the representation $\Gamma_{12'}^-$ in the notation of Dresselhaus *et al.*[18] The expressions (11) for $F$, $H_2$, and $A'$ imply neglecting coupling to the high-energy $f$-like bands. We emphasize that $f$ partial waves are not included in the LMTO calculations anyway. The first term in $A'$ is symmetry allowed in zinc-blende-type materials due to the lack of inversion symmetry. This term is, of course, zero in diamond-type materials. The second term in $A'$ is expected to give the dominant contribution since the $\Gamma_1^c$ and $\Gamma_{15}^{\prime c}$ conduction bands are relatively close in energy; see Fig. 2 (the energy difference $E_{\Gamma_{15}^{\prime c}} - E_{\Gamma_1^c}$ is close to the energy difference $E_{\Gamma_1^c} - E_{\Gamma_{15}^v}$).

Following the determination of the matrix elements $F$, $G$, and $M$ we obtain the Luttinger parameters $\gamma_1$, $\gamma_2$, $\gamma_3$, $\kappa$, and $q$ from[24]

$$\gamma_1 = -\frac{1}{3}(2F + 4G + 4M) - 1 + q ,$$
$$\gamma_2 = -\frac{1}{6}(2F + 4G - 2M) - q ,$$
$$\gamma_3 = -\frac{1}{6}(2F - 2G + 2M) + q ,$$
$$\kappa = -\frac{1}{3}\gamma_1 + \frac{2}{3}\gamma_2 + \gamma_3 - \frac{2}{3} - \frac{9}{2}q ,$$
$$q = \frac{2}{9}\frac{H_1^2 \Delta_0'}{Q^2} . \qquad (13)$$

Note that for materials with very small spin-orbit coupling (as, e.g., 3$C$-SiC), the parameter $q$ can be neglected in the expressions above.

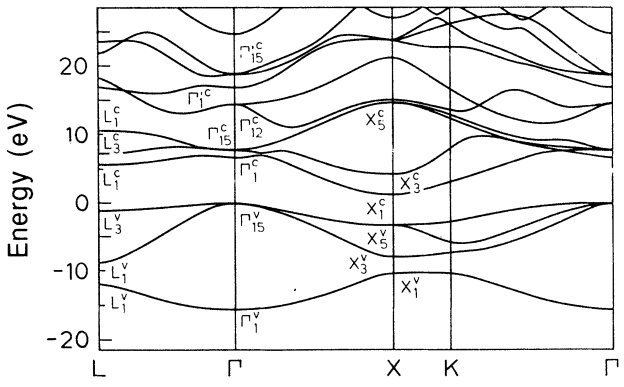


FIG. 2. Band structure of 3$C$-SiC as calculated from the LMTO method in the local-density approximation.

## IV. ESTIMATE OF $P'$

In the present work, $P'$ has been estimated in two ways. The second term in the expression for $A'$ (proportional to $S^2$) was calculated for Si by Cardona and Pollak,[25] and for C in a previous publication by us.[17] Taking the average value as an estimate for the second term of $A'$ in SiC and using expression (5), we obtain $P'$ from our LMTO calculations of $m_4$ in the local-density approximation. This is possible since $P$ is known once

the valence band effective masses are determined from the LMTO LDA ($P$ is given by the parameters $L$, $M$, and $N$). In this way we obtain $|P'| = 0.017$ a.u. However, in our calculations of the band structure of SiC using a $16 \times 16$ $\vec{k} \cdot \vec{p}$ model, we employ $P' = -0.0123$ a.u., obtained from the spin-splitting results (see later sections). Compared with the value found for the III-V or II-VI compounds ($P'/P \approx 0.3$) our value of $P'/P$ for SiC is negligibly small.

In Refs. 26 and 27, $P'$ was also estimated by a linear combination of atomic orbitals approach [see Eqs. (16) and (17) below] based on the assumption that the interatomic nearest-neighbor contributions are much larger than intra-atomic $s$-$p$ matrix elements. This is a good approximation for Si, Ge, and $\alpha$-Sn. For diamond, due to the lack of core $p$ electrons, the intra-atomic contributions are large and predictions by this method become rather unreliable, in both magnitude and sign.

## V. ESTIMATES OF $\Delta^-$ IN SiC

The spin-orbit coupling parameter $\Delta^-$ is defined as[11]

$$\Delta^- = 3\left\langle \left(\frac{3}{2}\frac{3}{2}\right)_v \middle| H_{\rm so} \middle| \left(\frac{3}{2}\frac{3}{2}\right)_c \right\rangle , \tag{14}$$

where $|\left(\frac{3}{2}\frac{3}{2}\right)_v\rangle$ [$|\left(\frac{3}{2}\frac{3}{2}\right)_c\rangle$] represents the eigenvector of the $\Gamma_{15}^v$ [$\Gamma_{15}^c$] eigenstate. According to the phase convention of Fig. 1 (both eigenstates are chosen real), $\Delta^-$ is real. The magnitude of $\Delta^-$ can be determined by performing calculations for the $\Gamma_{15}^v$ and the $\Gamma_{15}^c$ states both with and without the inclusion of spin-orbit interaction. In the absence of $\Delta^-$ coupling, the $\Gamma_{15}$ bands split into $J = 3/2$ and $1/2$ ($\Gamma_8$ and $\Gamma_7$) components, the shifts being in the ratio 2:1. Including second-order perturbation terms, these shifts deviate slightly from the ratio 2:1 characterized by $\Delta^-$ as follows:[11]

$$\delta\left(\frac{3}{2}\right) = \frac{\Delta_0}{3} - \left(\frac{\Delta^-}{3}\right)^2 \Big/ E_0' ,$$
$$\delta\left(\frac{1}{2}\right) = -\frac{2\Delta_0}{3} - \left(\frac{2\Delta^-}{3}\right)^2 \Big/ E_0' . \tag{15}$$

Here $\Delta_0$ is the spin-orbit splitting that one would have if $\Delta^- = 0$. Inserting into Eq. (15), the values $\delta\left(\frac{3}{2}\right) = 4.8$ meV and $\delta\left(\frac{1}{2}\right) = -9.6$ meV, we find $\Delta_0 = 14.4$ meV and $|\Delta^-| = 26$ meV. $\Delta_0'$ was determined in a similar way to be 69.6 meV.

We also performed a tight-binding estimate of $\Delta^-$. Assuming that the $\Gamma_{15}^v$ and the $\Gamma_{15}^c$ wave functions are obtained as bonding and antibonding linear combinations of the Si and C $p$ states, we have[26,27]

$$|\Gamma_{15}^v\rangle = \alpha\,|\,{\rm C}\rangle + \beta\,|\,{\rm Si}\rangle ,$$
$$|\Gamma_{15}^c\rangle = \beta\,|\,{\rm C}\rangle - \alpha\,|\,{\rm Si}\rangle . \tag{16}$$

The $s$ states are distinguished from the $p$ states by a prime. We can then write for the antibonding $\Gamma_1^c$ state

$$|\Gamma_1^c\rangle = \beta'\,|\,{\rm C}'\rangle - \alpha'\,|\,{\rm Si}'\rangle . \tag{17}$$

In the following discussion, it is convenient to introduce the parameters $\eta = \frac{\alpha}{\beta}$ and $\eta' = \frac{\alpha'}{\beta'}$. Referring to Eq. (16) and Fig. 1, we point out that $|\,{\rm C}\rangle$ and $|\,{\rm Si}\rangle$ are chosen to have the positive lobe to the right, so that the coefficients satisfy $\alpha > 0$ and $\beta < 0$. The ratio of $\alpha$ and $\beta$ can be obtained from Harrison[28]

$$\eta = \frac{-2H_{xx}}{E_p^{\rm C} - E_p^{\rm Si} + \left[(E_p^{\rm C} - E_p^{\rm Si})^2 + 4H_{xx}^2\right]^{1/2}} , \tag{18}$$

where $E_p^{\rm C}$ and $E_p^{\rm Si}$ are the atomic term values that appear on the diagonal of the tight-binding Hamiltonian. $H_{xx}$, the composite matrix element, is a function of the bond length $d$ and can be written as[28,29]

$$H_{xx} = \frac{4}{3}V_{pp\sigma} + \frac{8}{3}V_{pp\pi} = \frac{1.28}{d^2} . \tag{19}$$

The equation is based on parameters derived from a $sp^3s^*$ tight-binding model. We calculated $\eta$ from Eq. (18) to be $-1.82$ using the term values of Harrison.[30] This results in a bonding wave function $\Gamma_{15}^v$ that is more anionlike (C has a larger electronegativity than Si. We therefore denote C as the anion and Si as the cation). The term energies given by Harrison are free-atom-like, not self-consistent, and independent of crystal volume. A similar calculation, but based on self-consistent term energies extracted from LMTO calculations[31] (including downfolding of the $d$ orbitals and empty-sphere orbitals) for the SiC compound, yields the value, $\eta = -1.34$. The difference observed here between the LMTO and the Harrison estimates emphasizes the importance of self-consistent calculations.

The ratio $\eta' = \frac{\alpha'}{\beta'}$ (both of the same sign) is given by

$$\eta' = \frac{-2V_{ss\sigma}}{E_s^{\rm C} - E_s^{\rm Si} + \left[(E_s^{\rm C} - E_s^{\rm Si})^2 + 4V_{ss\sigma}^2\right]^{1/2}} , \tag{20}$$

where

$$V_{ss\sigma} = -\frac{1.32}{d^2} . \tag{21}$$

In this case, Harrison's value is $\eta' = 2.09$ and the LMTO value is 2.02,[31] i.e., the $\Gamma_1^c$ conduction electrons reside more on the Si side corresponding to a cationlike antibonding wave function $\Gamma_1^c$. In III-V compounds, the $\Gamma_1^c$ conduction electrons are *always* cationlike. Earlier calculations indicate, however, for GeSi[26] that the $\Gamma_1^c$ conduction electrons are anionlike, even though the assignment of Si as an anion in the GeSi material system is somewhat uncertain.

The spin-orbit parameters $\Delta_0$, $\Delta_0'$, and $\Delta^-$ (and their signs) can now be estimated from the expressions[11]

$$\Delta^- = \alpha\beta\left[\Delta_0({\rm C}) - \Delta_0({\rm Si})\right] ,$$
$$\Delta_0 = \alpha^2\Delta_0({\rm C}) + \beta^2\Delta_0({\rm Si}) ,$$
$$\Delta_0' = \beta^2\Delta_0({\rm C}) + \alpha^2\Delta_0({\rm Si}) . \tag{22}$$

Equation (22) gives $\Delta^- = 18.2$ meV, $\Delta_0 = 19.6$ meV, and $\Delta_0' = 30.4$ meV using the LMTO value of $\eta = \frac{\alpha}{\beta} = -1.34$, (Ref. 31) and renormalized atomic spin-orbit splittings for diamond [$\Delta_0({\rm C}) = 0.006$ eV] and silicon [$\Delta_0({\rm Si}) =$

0.044 eV].[32] The spin-orbit splittings obtained here are in reasonable agreement with the above LMTO results. It should be emphasized, however, that the mixing of $d$ states into the $\Gamma_{15}$ states (especially the $\Gamma_{15}^c$ states) has not been included in the tight-binding expressions.

## VI. NUMERICAL RESULTS

The band structure of cubic SiC calculated within the local-density approximation using the self-consistent relativistic LMTO method is shown in Fig. 2. We emphasize that the adjusting potential method, using $\delta$-like potentials centered at the atoms to shift the $s$-like states[33] and later extended to include potentials shifting the $p$-like states,[34] is not able to reproduce agreement with experimental results for band gaps of SiC at the high symmetry $\Gamma$, $X$, and $L$ points.[35] Therefore we apply here the LMTO band structure calculations in the local-density approximation to obtain the momentum matrix elements. Note that these matrix elements, necessary for the evaluation of effective masses, Luttinger parameters, spin splittings, and the detailed band structure of the upper valence and the lower conduction bands by means of a $16 \times 16$ $\vec{k} \cdot \vec{p}$ Hamiltonian analysis, are expected to be well described by the LDA even for materials with a large direct band gap, such as 3C-SiC. This follows from the weak influence of quasiparticle corrections to the Hamiltonian in the $GW$ approach on the LDA wave functions.

In Table I, we show the calculated energies at the high symmetry points $\Gamma$, $X$, and $L$ with the LMTO method in the local-density approximation. The results of Rohlfing *et al.*[16], obtained with the quasiparticle $GW$ calculations and experimental data are also listed.

The finer structure around $k = 0$ in the [100], [110], and [111] directions of the Brillouin zone was examined to obtain the effective masses. By fitting a straight line to the calculated electronic energies versus $k^2$ in the immediate vicinity of point $\Gamma$, the slopes determine the LDA effective masses for the different directions. In agreement with the $\vec{k} \cdot \vec{p}$ results we find that the effective mass of the $s$-like conduction band $\Gamma_1^c$, $m_4$, is isotropic whereas the $\Gamma_{15}^v$ hole masses show a strong anisotropy given by the parameters $L$, $M$, $N$ of Dresselhaus *et al.* or, equivalently, the Luttinger parameters $\gamma_1$, $\gamma_2$, and $\gamma_3$.

In Table II the LDA effective masses calculated by the LMTO method and the corrected effective masses obtained from our LMTO and $\vec{k} \cdot \vec{p}$ calculations [using the experimental result for $E_{\Gamma_1^c}$ (7.4 eV) (Ref. 39) and the $GW$ result for $E_{\Gamma_{15}^c}$ (8.35 eV) (Ref. 16)] are listed. We have shown both the masses near $\Gamma$ for $\Delta_0 = 0$ ($m_1$, $m_2$, $m_3$, $m_4$) obtained directly from our calculations and those for $\Delta_0 \neq 0$ ($m_{\rm so}$, $m_{\rm lh}$, $m_{\rm hh}$, $m_c$) calculated with the expressions (2)–(5) and (6)–(9), respectively. The corrected mass values given in Table II were calculated using the following scheme: First, we determine the matrix elements $P^2$, $Q^2$, $R^2$, and $S^2$ in (11) using the LDA energies (Table I) and the LDA effective masses (Table II).

TABLE I. Energies (in eV) of SiC at the symmetry points $\Gamma$, $X$, and $L$ and the indirect energy gap.

| | LMTO (LDA) | $GW$, Rohlfing *et al.* (Ref. 16) | Expt. |
|---|---|---|---|
| $E_{\Gamma_1^v}$ | −15.49 | −16.54 | |
| $E_{\Gamma_{15}^v}$ | 0.0 | 0.0 | 0.0 |
| $E_{\Gamma_1^c}$ | 6.74 | 7.24 | 7.4[a] |
| $E_{\Gamma_{15}^c}$ | 7.80 | 8.35 | 7.75[b] |
| $E_{\Gamma_{12}^c}$ | 14.54 | | |
| $E_{\Gamma_{15}'^c}$ | 18.79 | | |
| $E_{\Gamma_1'^c}$ | 16.92 | | |
| $E_{X_1^v}$ | −10.36 | −11.46 | |
| $E_{X_3^v}$ | −7.87 | −8.65 | |
| $E_{X_5^v}$ | −3.23 | −3.65 | −3.6,[b] −3.4[a] |
| $E_{X_1^c}$ | 1.40 | 2.18 | 2.39[b] |
| $E_{X_3^c}$ | 4.36 | 5.48 | 5.5,[b] 4.7[b] |
| $E_{X_5^c}$ | 14.66 | 15.91 | |
| $E_{L_1^v}$ | −11.84 | −12.93 | |
| $E_{L_1^v}$ | −8.69 | −9.43 | |
| $E_{L_3^v}$ | −1.04 | −1.22 | −1.16[b] |
| $E_{L_1^c}$ | 5.69 | 6.46 | 4.2[c] |
| $E_{L_3^c}$ | 7.35 | 8.52 | 8.5[b] |
| $E_{L_1^c}$ | 10.66 | 11.97 | |
| $E_{\rm gap}^{\rm ind}$ | 1.20 | 2.18 | 2.39[b] |

[a]From Ref. 39.

[b]From Ref. 23.

[c]From Ref. 23 (this corresponds to $E_{L_1^c} - E_{L_3^v} = 5.36$ eV). In Ref. 39, $E_{L_1^c} - E_{L_3^v}$ was found to be 7.5 eV.

TABLE II. Effective masses of the $p$-like valence band states and lower $s$-like conduction band state ($m_4$) of $3C$-SiC calculated in the present work. $m_1$, $m_2$, and $m_3$ represent the hole masses in the absence of spin-orbit splitting while $m_{hh}$, $m_{lh}$, and $m_{so}$ represent the physically more meaningfull hole masses including the spin-orbit splitting at Γ. The LMTO-corrected effective masses in column 3 are calculated from the LDA effective masses in column 2 corrected for the discrepancy between the experimental and the $GW$ and calculated energy gaps.

| | LMTO (LDA) | LMTO Corrected |
|---|---|---|
| $m_1^{100}$ | 0.379 | 0.410 |
| $m_1^{111}$ | 0.208 | 0.227 |
| $m_1^{110}$ | 0.285 | 0.255 |
| $m_2^{100}$ | 0.595 | 0.470 |
| $m_2^{111}$ | 1.68 | 1.91 |
| $m_2^{110}$ | 0.596 | 0.662 |
| $m_3^{100}$ | 0.595 | 0.662 |
| $m_3^{111}$ | 1.68 | 1.91 |
| $m_3^{110}$ | 19.32 | 33.3 |
| $m_4$ | 0.412 | 0.449 |
| $m_{so}$ | 0.497 | 0.545 |
| $m_{hh}^{100}$ | 0.593 | 0.662 |
| $m_{hh}^{111}$ | 1.68 | 1.91 |
| $m_{hh}^{110}$ | 1.35 | 1.46 |
| $m_{lh}^{100}$ | 0.434 | 0.470 |
| $m_{lh}^{111}$ | 0.318 | 0.321 |
| $m_{lh}^{110}$ | 0.345 | 0.339 |
| $m_c$ | 0.414 | 0.449 |

As mentioned earlier, these matrix elements are solely determined by the wave functions, which are expected to be well described by the local-density approximation. Next, combining $P^2$, $Q^2$, $R^2$, $S^2$, and the experimental or the $GW$ energy values mentioned above, we obtain the renormalized (or corrected) effective masses in column 2 of Table II.

In Table III we list the matrix elements and other band parameters obtained from the LMTO and $\vec{k}\cdot\vec{p}$ calculations.

In Table IV, the corrected Luttinger parameters are given together with transverse and longitudinal effective masses at the $X_1$ conduction band minimum. For comparison, previously published results are also shown.[1,6,5]

TABLE III. Matrix elements (in atomic units) and other band parameters at Γ obtained by the LMTO and $\vec{k}\cdot\vec{p}$ calculations.

| | |
|---|---|
| $F$ | −1.018 |
| $M$ | −1.212 |
| $G$ | −0.351 |
| $P$ | 0.527 |
| $P'$ | −0.0123 |
| $P'''$ | 0.7101 |
| $Q$ | 0.6216 |
| $R$ | 0.4336 |
| $S$ | 0.4196 |

The Luttinger parameters may, of course, be derived directly from the corrected effective hole masses given in Table II. We also checked for the wave function composition of the $X_1^c$ state and found it to be $s$ like on the C atom and $p$ like on the Si atom. The opposite situation was found for the $X_3^c$ state.[40]

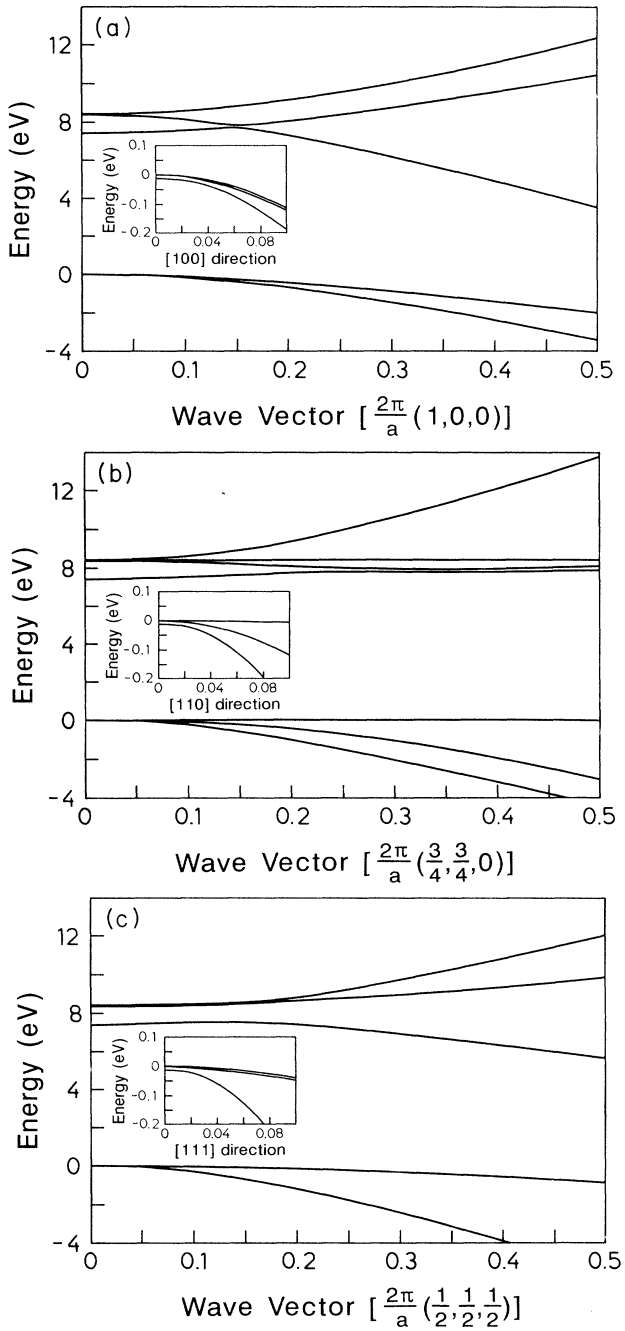


FIG. 3. The upper valence and lower conduction band structure of $3C$-SiC as calculated from the 16 × 16 $\vec{k}\cdot\vec{p}$ model in the [100], [110], and [111] directions. The zero of energy has been chosen at the $\Gamma_8^v$ state. The inset shows the detailed band structure of the upper valence band close to the Γ point.

TABLE IV. Luttinger parameters for 3$C$-SiC, transverse ($m_\perp$) and longitudinal ($m_\parallel$) effective masses at the conduction band minimum ($X$), and spin-orbit energies in eV.

| | Present | Bimberg *et al.* (Ref. 5) | Kono *et al.*[1] | Kaplan *et al.* (Ref. 6) |
|---|---|---|---|---|
| $\gamma_1$ | 1.820 | 2.817 | | |
| $\gamma_2$ | 0.155 | 0.508 | | |
| $\gamma_3$ | 0.648 | 0.860 | | |
| $\kappa$ | −0.52 | −0.41 | | |
| $m_\perp$ | 0.29 | | 0.25 ± 0.01 | 0.247 |
| $m_\parallel$ | 0.60 | | 0.67 ±0.01 | 0.667 |
| $\Delta_0$ | $14.4 \times 10^{-3}$ | $10.2 \times 10^{-3}$ | | |
| $\Delta_0'$ | $69.6 \times 10^{-3}$ | | | |
| $\Delta^-$ | $26.0 \times 10^{-3}$ | | | |

Following the determination of the matrix elements $P, P', P''', Q, R, S$, and using the parameters $E_0$, $\Delta_0$, $E_0'$, $\Delta_0'$, $E_0'''$, $C_k$, $C_k'$, $\gamma_1$, $\gamma_2$, and $\gamma_3$ (all obtained from our LMTO calculations), we are in a position to perform detailed band structure calculations at the $\Gamma$ point using a $16 \times 16$ $\vec{k} \cdot \vec{p}$ Hamiltonian involving matrix elements between six $\Gamma_{15}^v$, six $\Gamma_{15}^c$, two $\Gamma_1^c$, and two $\Gamma_1'^c$ wave functions. As a basis we take the linear combinations of these states, which correspond to $(\frac{3}{2}, \pm\frac{3}{2})$, $(\frac{3}{2}, \pm\frac{1}{2})$, and $(\frac{1}{2}, \pm\frac{1}{2})$ angular-momentum states with $z$ along [001] as the quantization axis. Portions of the Hamiltonian can be found in Table I of Ref. 11 (between the $\Gamma_7^c, \Gamma_8^c$ and the $\Gamma_7^v, \Gamma_8^v, \Gamma_6^c$ states) and in the Appendix of Ref. 41 (the "diagonal" matrix connecting the $\Gamma_{15}^v$ states with themselves).

In Fig. 3 we show the upper valence and the lower conduction band structure in the [100], [110], and [111] directions calculated with the $16 \times 16$ $\vec{k} \cdot \vec{p}$ Hamiltonian *using the experimental direct gap values* (along in the [100] direction the lowest conduction band is not well represented, a fact that signals the incorrectness of the $16 \times 16$ $\vec{k} \cdot \vec{p}$ basis for $k \geq \frac{\pi}{a_0}$). In this way, we obtain information about the $\Gamma_{15}^c$ conduction band effective masses. The effective masses are listed in Table V for the three directions [100], [110], and [111]. These values can also be obtained from a $\vec{k} \cdot \vec{p}$ analysis in the upper $s$-like conduction band states ($\Gamma_1'^c$) and the $p$-like conduction band states ($\Gamma_{15}^c$) similar to that presented above in the lower $s$-like conduction and the upper $p$-like valence band states. Furthermore, we conclude from Fig. 3 that the valence band maximum of 3$C$-SiC occurs at $\Gamma$. The same conclusion was found in the case of semiconducting diamond C, contrary to a suggestion in Ref. 42.

TABLE V. Effective masses of the $\Gamma_{15}^c$ conduction band states close to the $\Gamma$ point in the [100], [110], and [111] directions.

| | [100] | [110] | [111] |
|---|---|---|---|
| $m_{\rm se}^c$ | 2.65 | 2.65 | 2.65 |
| $m_{\rm le}^c$ | 0.402 | 0.668 | 1.20 |
| $m_{\rm he}^c$ | 0.561 | 1.26 | 8.26 |

## VII. INVERSION-ASYMMETRY-INDUCED SPIN SPLITTING IN SiC

### A. Cubic terms along [110]

All bands along [110] are split by spin-orbit interaction in zinc-blende-type materials. The splitting energy can be written for small $k$ as[11,19]

$$\Delta E = \gamma k^3 , \tag{23}$$

where $\gamma$ is positive if the $\Sigma_4$ state is above the $\Sigma_3$ state. We shall use $\gamma$ with the subscripts $c$ ($s$-like conduction), hh (heavy hole), lh (light hole), sh (split hole), he (heavy electron), le (light electron), and se (split electron). In Figs. 4–8, the splittings near $\Gamma$ are depicted.

We have extracted the different $\gamma$'s from our LMTO data by fitting the energy difference $\Delta E$ of the split bands to $k^3$ using a very dense mesh close to the $\Gamma$ point. When required by symmetry, we added a linear term in $k$ whose coefficient is also found from the hh and he splittings along [111] as discussed in Sec. VII C. In Table VI, the calculated $\gamma$'s (in units of eV Å$^3$) are listed. Also given in the table are $\gamma$ values obtained from third-order (in $\vec{k} \cdot \vec{p}$) perturbation theory from states that exactly include $\Delta_0$,

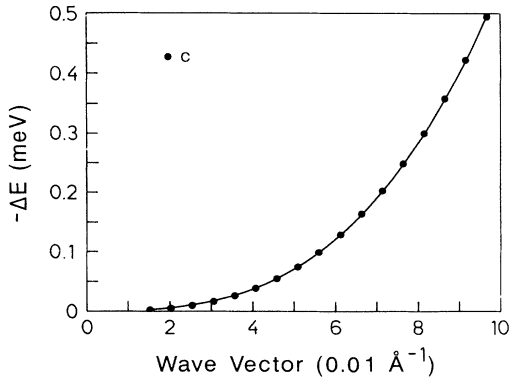


FIG. 4. Spin splitting along [110], close to $\Gamma$, of the first $s$-like conduction band as calculated with the LMTO method.

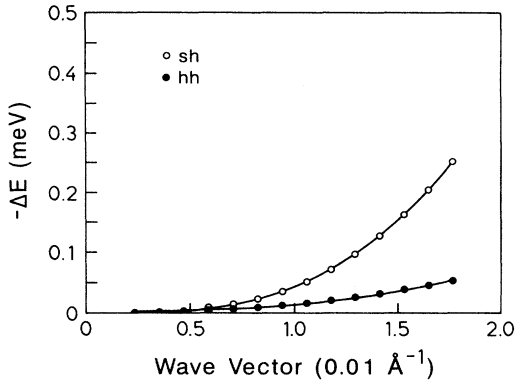


FIG. 5. Spin splitting along [110], close to Γ, of the hh and sh bands as calculated with the LMTO method.

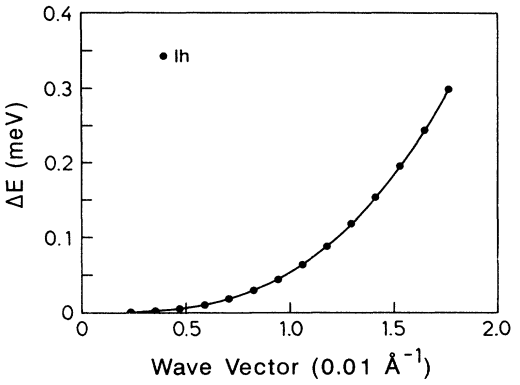


FIG. 6. Spin splitting of the lh band along [110] and close to Γ. A small linear term is found from the fit opposite to the sign of the cubic contribution.

$\Delta_0'$, and $\Delta^-$. The signs of the splittings are taken from the $\vec{k}\cdot\vec{p}$ calculations.

### 1. $\Gamma_1^c$ band along [110]

According to fourth-order perturbation theory (3 times $\vec{k}\cdot\vec{p}$ and once $H_{so}$), $\gamma_c$ is given by[11]

$$\gamma_c = A + B + C + D\,, \tag{24}$$

where

$$A = \frac{4}{3}PP'Q\frac{\Delta_0}{3E_0(E_0+\Delta_0)}\left[\frac{2}{E_0'-E_0+\Delta_0'} + \frac{1}{E_0'-E_0}\right],$$

$$B = \frac{4}{3}PP'Q\frac{\Delta_0'}{3(E_0'-E_0)(E_0'-E_0+\Delta_0')}\left[\frac{2}{E_0} + \frac{1}{E_0+\Delta_0}\right],$$

$$C = -\frac{4}{3}\frac{P^2Q\Delta^-}{\bar{E}_0^2(\bar{E}_0'-E_0)}\,,$$

$$D = -\frac{4}{3}\frac{P'^2Q\Delta^-}{\bar{E}_0(\bar{E}_0'-E_0)^2}\,. \tag{25}$$

Here $E_0' = E_{\Gamma_7^c} - E_{\Gamma_8^v}$ and the bar above $E_0$ and $E_0'$ represents an average of the two spin-orbit split components with weight two for $\Gamma_7$ and 1 for $\Gamma_8$. Note that $\gamma_c$ (and the other spin-splitting coefficients) vanishes for diamond-type crystals, where $P' = \Delta^- = 0$. The magnitude and the sign of $P'$ are extracted by comparing our LMTO results for the $\Gamma_1^c$ spin splitting ($\gamma_c = -0.54$ eV Å$^3$) with the $\vec{k}\cdot\vec{p}$ expression [Eq. (25)] using LDA energy values listed in Table I. Since the spin splitting is very sensitive to the value (and sign) of $P'$, we expect $P' = -0.0123$, obtained in this way, to be rather accurate. As a consequence of the very small values of the spin-orbit parameters $\Delta_0$, $\Delta_0'$, and $\Delta^-$ obtained from the LMTO calculations and the small value of $P'$, the terms $A$, $B$, $C$, and $D$ contribute little to $\gamma_c$. The corresponding values for the spin-splitting parameter $\gamma_c$ in the group-IV compounds SnGe (Ref. 27) and GeSi (Ref. 26) are −272.67 a.u. and −7.1 a.u., respectively.

### 2. $\Gamma_{15}^v$ band along [110]

The second-order $\vec{k}\cdot\vec{p}$ interaction with $\Gamma_1$ proportional to $2L + 4M$ give the main contribution to the band curvatures [Eqs. (7) and (8)]. This interaction is therefore nearly isotropic and the [110] wave functions of $\Gamma_8^v$ still can be assumed to have the form of angular-momentum functions $|\, j, m_j\rangle = \left(\frac{3}{2},\pm\frac{3}{2}\right), \left(\frac{3}{2},\pm\frac{1}{2}\right)$ corresponding to

TABLE VI. Values for the cubic splitting coefficients ($\gamma$'s in eV Å$^3$ ) and the linear splitting coefficients ($C_k$ and $C_k'$ in meV Å ) of 3$C$-SiC. The pure LMTO results are compared to those obtained by $\vec{k}\cdot\vec{p}$ theory using the value $P' = -0.0123$. The values listed in the second (third) row are calculated using LDA (corrected) energies.

| | $\gamma_c$ | $\gamma_{lh}$ | $\gamma_{sh}$ | $\gamma_{se}$ | $\gamma_{le}$ | $\lvert\gamma_{he}\rvert$ | $C_k$ | $C_k'$ |
|---|---|---|---|---|---|---|---|---|
| LMTO | −0.54 | 54.7 | −46.8 | −0.13 | 0.32 | 0.05 | −0.10 | +0.04 |
| $\vec{k}\cdot\vec{p}$ (LDA) | −0.54 | 38.4 | −37.9 | −1.52 | 1.71 | | | |
| $\vec{k}\cdot\vec{p}$ (corrected) | −0.50 | 32.7 | −32.2 | −1.91 | 2.11 | | | |

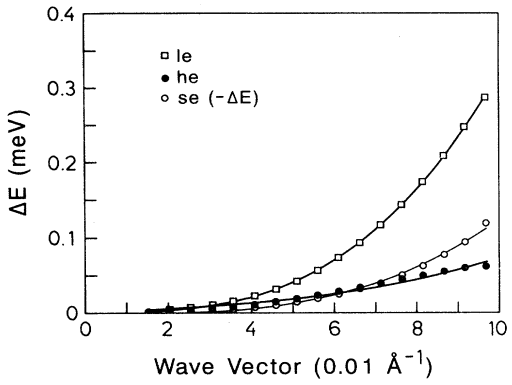


FIG. 7. Detail of the spin splitting of the lowest $p$-like conduction band states along [110], close to the $\Gamma$ point.

hh-like and lh-like states, respectively, with quantization axis in the [110] direction.

Perturbation theory up to fourth-order predicts $\gamma_{\rm hh}$ to be zero, but terms of order higher than $k^3$ (such as $k^5$) contribute to the splitting. In fact, from Fig. 5 we observe contributions from such higher-order terms. The coefficient for the lh band is given by[11]

$$\gamma_{\rm lh} = -\frac{4PP'Q}{3E_0\bar{E}_0'} + \frac{4P^2Q\Delta^-}{3E_0\bar{E}_0'\Delta_0} + \frac{2Q^3\Delta^-}{3E_0'^2\Delta_0} . \qquad (26)$$

The lh curve is shown in Fig. 6. From the LMTO calculations, we find the value $\gamma_{\rm lh} = 54.7$ eV Å$^3$. In addition, a small negative linear coefficient is obtained using a $Ak^3 + Bk$ fit. The linear term can be determined more precisely from spin splittings of the hh band along [111], where no cubic terms contribute according to $\vec{k}\cdot\vec{p}$ theory. We shall discuss this later. The $\gamma_{\rm sh}$ coefficient for the split-off band can be obtained from Eq. (26) by adding the corresponding so splitting $\Delta_0$ to the energy $E_0$ in the denominator and reversing the sign. In this case we find the values $\gamma_{\rm sh} = -46.8$ eV Å$^3$ (LMTO) and $\gamma_{\rm sh} = -37.9$ eV Å$^3$ ($\vec{k}\cdot\vec{p}$).

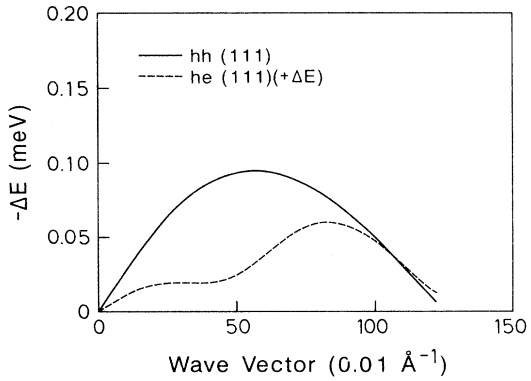


FIG. 8. Spin splittings of the hh (solid) and he (dashed) $\Gamma_8^{v,c}$ bands in 3$C$-SiC for $\vec{k}$ along [111] as calculated with the LMTO method.

### 3. $\Gamma_{15}^c$ band along [110]

The $\Gamma_7^c$ bands are given by $\left(\frac{1}{2},\pm\frac{1}{2}\right)$ wave functions with [110] being the quantization axis. The parameter $P''' = i\langle\Gamma_{15}^c \mid p_x \mid \Gamma_1'^c\rangle$, which enters into the expression for $\gamma_{\rm se}$ and $\gamma_{\rm le}$, was determined to be 0.7101 a.u. by combining our LMTO calculations with $\vec{k}\cdot\vec{p}$ expressions, as already mentioned. From Ref. 11, we have

$$\gamma_{\rm se} = -\frac{4PP'Q}{3(E_0'-E_0)(E_0'+2\Delta_0/3)} + \frac{4P'^2Q\Delta^-}{3(E_0'-E_0)(E_0'+2\Delta_0/3)\Delta_0'} + \frac{2Q^3\Delta^-}{3(E_0'+2\Delta_0/3)^2\Delta_0'} - \frac{4P'''^2Q\Delta^-}{3(E_0'''-E_0')(E_0'+2\Delta_0/3)\Delta_0'} . \qquad (27)$$

The fourth term is due to the interaction with the $\Gamma_1'^c$ band. If we assume that the $\Gamma_8^c$ states along [110] are predominantly $\left(\frac{3}{2},\pm\frac{3}{2}\right)$ (for he) and $\left(\frac{3}{2},\pm\frac{1}{2}\right)$ (for le), the expression for $\gamma_{\rm le}$ would be obtained from Eq. (27) by adding $\Delta_0'$ to $E_0'$ and reversing all signs. The LMTO and $\vec{k}\cdot\vec{p}$ results for $\gamma_{\rm se}$ and $\gamma_{\rm le}$ are given in Table VI. Furthermore, we find from Fig. 7 that the spin splitting of the he bands exhibits a very small but nonzero value for $\gamma_{\rm he}$ (found to be 0.05 eV Å$^3$). From $\vec{k}\cdot\vec{p}$ theory, this coefficient should be zero to third order in $k$, similar to the case of the hh bands.

## B. Discussion

Overall we find reasonable agreement between the values of the parameters derived from our LMTO calculations and those obtained with $\vec{k}\cdot\vec{p}$ perturbation theory (Table VI). The calculations are therefore consistent and support our estimates of $\Delta^-$, $P'$, and $P'''$. Moreover, we conclude that the approximations made (pure $J_z$ eigenstates, fourth-order perturbation theory, and matrix elements determined from the LMTO LDA) are valid. However, some discrepancy is observed between the LMTO and the $\vec{k}\cdot\vec{p}$ results for the $\Gamma_{15}^c$ bands, which signals a partial breakdown of the approximation of pure $J_{\bar{z}}$ states.

## C. Terms linear in $k$

The existence of spin splittings linear in $k$ in zinc-blende-type materials has been known for a long time.[18,19] Measurements using magneto-optical[43] and polariton-scattering techniques[44,45] yield information about these linear splittings. Here we shall consider the splittings in the [111] and the [110] directions. For the sh,

se, and $s$-conduction ($c$) bands there are no linear terms, whereas the lh and le bands only show a linear splitting along [110]. We designate the coefficients by $C_k$ for the valence bands and $C'_k$ for the conduction bands.[11,26,46]

It has been demonstrated[11] that the main contribution to $C_k$ and $C'_k$ usually is the second-order interaction, bilinear in $\vec{k}\cdot\vec{p}$ and in the spin-orbit Hamiltonian $H_{so}$ between the $\Gamma_8^v$ and the uppermost $d$ core levels ($\Gamma_{12}$ intermediate states), and that the contribution from the $k$-dependent spin-orbit Hamiltonian vanishes. For SiC the situation is different, since there are no core $d$ states in Si and C. We return to this point later. In Fig. 8 we present the splittings of the hh and he bands along [111]. The symmetries are $\Lambda_5$ and $\Lambda_4$, respectively. For small $k$, the splitting along [111] is linear (no cubic terms) and is related to $C_k$ for the hh bands by[18,19,46]

$$E(\Lambda_5) - E(\Lambda_4) = 2\sqrt{2}C_k k \ . \tag{28}$$

A similar relation holds, of course, for the he splitting with $C_k$ replaced by $C'_k$.

The magnitudes of $C_k$ and $C'_k$ are determined by fitting the slope for small $k$ and listed in Table VI. The signs of the linear coefficients were obtained from Figs. 5 and 7 relative to the cubic spin-splitting terms in the [110] direction. The absolute signs of $C_k$ and $C'_k$ are therefore determined from the signs of the cubic spin-splitting terms all ready found in the $\vec{k}\cdot\vec{p}$ calculations.

In the [110] direction, the splittings of the hh and the lh bands, assuming pure $\left(\frac{3}{2},\pm\frac{3}{2}\right)$ and $\left(\frac{3}{2},\pm\frac{1}{2}\right)$ symmetries and that the quadratic (effective-mass) splitting is larger than the linear one, are[18,19,46]

$$\begin{aligned} E_{\rm hh}(\Sigma_4) - E_{\rm hh}(\Sigma_3) &= \frac{3\sqrt{3}}{2}C_k k \ , \\ E_{\rm lh}(\Sigma_4) - E_{\rm lh}(\Sigma_3) &= \frac{\sqrt{3}}{2}C_k k \ . \end{aligned} \tag{29}$$

A similar relationship applies for the he and the le bands provided that $j$ and $m_j$ are still good quantum numbers. From the splitting in the [111] direction, we find $C_k = -0.10$ meV Å. We performed similar calculations using a fit of the type $Ak^3 + Bk$ in the [110] direction to obtain $C_k = -0.13$ meV Å (from the hh bands) and $C_k = -0.12$ meV Å (for the lh bands). The agreement is quite good and gives a measure of the validity of the assumption that hh and lh states are pure eigenstates of $J_z$. For $C'_k$ we find in a similar way the values +0.04 meV Å along [111] ($he$ bands), +0.06 meV Å along [110] (he bands), and +0.03 meV Å along [110] (le bands).

Earlier we mentioned that $C_k$ is mainly due to bilinear second-order perturbation terms, including $H_{\vec{k}\cdot\vec{p}}$ and $H_{so}$ with the $\Gamma_{12}$ (core $d$ levels) as intermediate states. Since there are no $d$ states in the cores of Si and C, these terms do not contribute to the linear splitting in SiC. $C_k$, however, can be understood as arising from the empty $\Gamma_{12}$ states through an expression of the type[26,27]

$$C_k = -A\frac{\Delta_{d,c}}{E_{\Gamma_8^v} - E_{d,c}} \ , \tag{30}$$

where we use for the cation $d$ states the empty $\Gamma_{12}$ states. In order to take into account the strong polarity of SiC we use for $A$ instead of the value 220 meV Å used for Ge and Si,[26] a value of −300 meV Å, [11] where the sign reversal is due to the fact that the $3d$ states of Si ($\Gamma_{12}$) are above the $\Gamma_{15}^v$ states. Using $\Delta_{3d}(Si)$ =0.005 (obtained by extrapolating the splittings of occupied $3d$ states[47]) we find

$$C_k = 300 \times \frac{0.005}{-15} = -\ 0.1 \text{ meV Å} \ , \tag{31}$$

in perfect agreement with the LMTO calculations. The $\Gamma_{12}$ (Si $3d$+ Ge $4d$) contribution, which should be much higher in zinc-blende-type SiGe, is probably the reason for the discrepancy between the LMTO value $C_k = -1.8$ meV Å in this material and the one obtained using only Ge core $3d$ states with the equivalent of Eq. (31) ($C_k = -\ 4.0$ meV Å ).

Concerning the value of $C'_k$, it is also reasonable to assume that it arises from the spin orbit and $p$ interactions of $\Gamma_{15}^c$ with $\Gamma_{12}$. Because of the lower content of carbon wave function in $\Gamma_{12}$, we expect the $C'_k$ should be lower than $C_k$ by about a factor of $\eta \approx -\ 3$. The smaller gap, however, should increase it by a factor of 2. Hence we expect $C'_k \approx -\frac{2}{3}C_k \approx +\ 0.07$ meV Å, also in reasonable agreement with the LMTO result $C'_k = +\ 0.04$ meV Å . The sign of $C'_k$ is consistent with Eq. (28) of Ref. 27. The $\Gamma_{12}$ interaction, not included in Eq. (7.8) of Ref. 11, is also probably responsible for the anomalous sign of $C'_k$ in InP given in Table XI of Ref. 11.

## VIII. IONICITY AND TRANSVERSE EFFECTIVE CHARGE IN SiC

Ionicity is a somewhat qualitative concept. According to Harrison, the polarity $\alpha_p$ is defined from tight-binding parameters of the $p$-valence orbitals as follows[28]:

$$\alpha_p = \frac{E_p^c - E_p^a}{\left[(E_p^c - E_p^a)^2 + 4H_{xx}^2\right]^{1/2}} \ , \tag{32}$$

where $E_p^c$ and $E_p^a$ are the term energies of the cation and the anion, respectively. For SiC one finds the value $\alpha_p$ =0.29 (LMTO with $\eta = -1.34$ according to Ref. 31) and $\alpha_p = 0.39$ (Harrison), much larger than the value found for GeSi (0.07).[26] For SnGe $\alpha_p$ has been calculated to be 0.20.[27] Although, following Harrison,[28] $p$-bonding $\rightarrow$ $p$-antibonding transitions are often believed to be responsible for global dielectric properties, one can argue that these may be better represented by transitions between bonding-antibonding $sp^3$ hybrids. We have thus evaluated the hybrid polarities $\alpha_h$ using the corresponding values of $E_h^c$, $E_h^a$, and $H_{h,xx}$ in Eq. (32). We find from the tight-binding parameters of Ref. 28 $\alpha_h = 0.61$, and from those of Ref. 31 $\alpha_h = 0.66$. (This value is obtained directly from the first-order tight-binding linear muffin-tin-orbital $sp^3$ two-site Hamiltonian. In Ref. 31, values are also given obtained from a Hamiltonian corrected to second order and reorthogonalized. This gives $\alpha_h = 0.47$.)

SiC is an infrared-active material and the optical phonon at $\Gamma$ is associated with an electric dipole moment represented by the transverse effective charge $e_T^*$. It is of interest to estimate $e_T^*$ to obtain insight into the infrared activity of $Si_nC_m$ superlattices and also the local modes of Si and C. Using the approximate expression for $e_T^*$ given in terms of $\alpha_p$ and the effective charge $Z^*$ (Ref. 28)

$$e_T^* = \frac{8}{3}\alpha_p(1-\alpha_p^2) + Z^* , \tag{33}$$

where $Z^*$ is 1.02 for SiC (Table 9.4 in Ref. 28), we find from Ref. 31 $e_T^* = 1.90$, which is much larger than that found for GeSi (0.09) and SnGe (0.47), but close to typical values for the III-V compounds. The experimental values given for $e_T^*$ in SiC is 2.69.[23] The value of the effective charge of carbon impurities in Si is 2.28 (after effective mass correction of the value 2.4 reported in Refs. 48 and 49). Using instead the hybrid parameters above, we find the effective charges $e_T^*$ =2.04 (Ref. 28) and $e_T^* = 2.01$ (2.00) using $\alpha_h = 0.66$ (0.47).[31] These values are somewhat closer to the experimental value than those obtained for $p$-orbital parameters. We emphasize that the positive sign of $e_T^*$ in SiC, and the corresponding negative charge in the C atom, is consistent with the large electronegativity of C compared to Si. Hence the phonon-induced infrared absorption, proportional to ${e_T^*}^2$, should be considerably higher for the local vibrational modes of C in Si, in comparison with phonon-induced infrared absorption in the group-IV compounds GeSi and SnGe.[26,27,50]

## IX. CONCLUSIONS

We have performed self-consistent relativistic (with the spin-orbit intercation treated as a perturbation) LMTO band structure calculations for SiC in the local-density approximation. Since the LMTO wave functions should not be significantly affected by quasiparticle corrections to the Hamiltonian, we determine matrix elements for the $\vec{k}\cdot\vec{p}$ Hamiltonian from the LMTO band structure. The matrix elements so obtained and the experimental energy gap values allow us to calculate renormalized effective masses and Luttinger parameters for SiC. These parameters are still poorly known for this material. A 16 $\times$ 16 $\vec{k}\cdot\vec{p}$ Hamiltonian calculation was performed using as input the above-mentioned parameters so as to obtain the detailed band structure of the upper valence and the lower conduction band states around the $\Gamma$ point in the [100], [110], and [111] directions. We find that the valence band maximum is located at the $\Gamma$ point (except for a small shift due to the linear $k$ terms), as in the case of semiconducting diamond,[17] and the conduction band minima at the $X$ point. Inversion-asymmetry-induced spin splittings have been discussed in terms of $\vec{k}\cdot\vec{p}$ and LMTO calculations. The cubic and linear spin-splitting coefficients were found to be much smaller than those obtained for SnGe and GeSi. (The $k^3$ spin-splitting terms should give rise to splittings linear in $k$ in $Si_nC_m$ superlattices provided that both $n$ and $m$ are odd.[51]) The ionicity and transverse effective charge were determined. The relatively high value of $e_T^*$ of SiC, compared to GeSi and SnGe, may lead to infrared absorption for sample thicknesses compatible with molecular-beam epitaxy growth techniques.

## ACKNOWLEDGMENT

M.W. acknowledges financial support from the Danish National Science Research Council (Contract No. 11-0855-1).

[1] J. Kono, S. Takeyama, H. Yokoi, N. Miura, M. Yamanaka, M. Shinohara, and K. Ikoma, Phys. Rev. B **48**, 10 909 (1993).
[2] J. Kono, N. Miura, S. Takeyama, H. Yokoi, N. Fujimori, Y. Nishibayashi, T. Nakajima, K. Tsuji, and M. Yamanaka, Physica B **184**, 178 (1993).
[3] S. Nishino, Y. Hazuki, H. Matsunami, and T. Tanaka, J. Electrochem. Soc. **ED-28**, 1235 (1981).
[4] M. Yamanaka, H. Daimon, E. Sakuma, S. Misawa, and S. Yoshida, Jpn. J. Appl. Phys. **61**, 599 (1987).
[5] D. Bimberg, M. Altarelli, and N. O. Lipari, Solid State Commun. **40**, 437 (1981).
[6] R. Kaplan, R. J. Wagner, H. J. Kim, and R. F. Davis, Solid State Commun. **55**, 67 (1985).
[7] W. H. Backes, P. A. Bobbert, and W. van Haeringen, Phys. Rev. B **49**, 7564 (1994).
[8] P. J. H. Denteneer and W. van Haeringen, Phys. Rev. B **33**, 2831 (1986).
[9] P. J. H. Denteneer and W. van Haeringen, Solid State Commun. **65**, 115 (1988).
[10] C. Cheng, R. J. Needs, and Volker Heine, J. Phys. C **21**, 1049 (1988).
[11] M. Cardona, N. E. Christensen, and G. Fasol, Phys. Rev. B **38**, 1806 (1988).
[12] O. K. Andersen, Phys. Rev. B **12**, 3060 (1975).
[13] D. Glötzel, B. Segal, and O. K. Andersen, Solid State Commun. **36**, 403 (1980).
[14] G. B. Bachelet and N. E. Christensen, Phys. Rev. B **34**, 5390 (1986).
[15] M. S. Hybertsen and S. G. Louie, Phys. Rev. B. **34**, 5390 (1986).
[16] M. Rohlfing, P. Krüger, and J. Pollmann, Phys. Rev. B **24**, 17 791 (1993).
[17] M. Willatzen, M. Cardona, and N. E. Christensen, Phys. Rev. B **50**, 18 054 (1994).
[18] G. Dresselhaus, A. F. Kip, and C. Kittel, Phys. Rev. **98**, 368 (1955).
[19] E. O. Kane, in *Physics of III-V Compounds*, edited by R. K. Willardson and A. C. Beer, Semiconductors and Semimetals Vol. 1 (Academic, New York, 1966), p. 75.
[20] K. Ya. Shtivel'man, Fiz. Tverd. Tela (Leningrad) **5**, 348 (1963) [Sov. Phys. Solid State **5**, 252 (1963)].

[21] W. R. L. Lambrecht and B. Segall, Phys. Rev. B **43**, 7070 (1991).
[22] W. R. L. Lambrecht, B. Segall, M. Methfessel, and M. van Schilfgaarde, Phys. Rev. B **44**, 3685 (1991).
[23] *Semiconductors Physics of Group IV Elements and III-V Compounds*, edited by K.-H. Hellwege and O. Madelung, Landolt-Börnstein, New Series, Group III, Vol. 22, Pt. a (Springer, Berlin, 1982).
[24] P. Lawaetz, Phys. Rev. B **4**, 3460 (1971).
[25] M. Cardona and F. H. Pollak, Phys. Rev. **142**, 530 (1966).
[26] U. Schmid, N. E. Christensen, and M. Cardona, Phys. Rev. B **41**, 5919 (1990).
[27] T. Brudevoll, D. S. Citrin, N. E. Christensen, and M. Cardona, Phys. Rev. B **48**, 17128 (1993).
[28] W. A. Harrison, *Electronic Structure and the Properties of Solids* (Freeman, San Fransisco, 1980).
[29] A. Blacha, H. Presting, and M. Cardona, Phys. Status Solidi B **126**, 11 (1984).
[30] W. A. Harrison, Phys. Rev. B **24**, 5835 (1981).
[31] W. R. L. Lambrecht and B. Segall, Phys. Rev. B **41**, 2832 (1990).
[32] J. C. Phillips, *Bonds and Bands in Semiconductors* (Academic, New York, 1973).
[33] N. E. Christensen, Phys. Rev. B **30**, 5753 (1984).
[34] T. Brudevoll, D. S. Citrin, M. Cardona, and N. E. Christensen, Phys. Rev. B **41**, 8629 (1993).
[35] Recently, Lambrecht *et al.* (Refs. 36 and 39) pointed out that literature values of experimental critical point energies may suffer from incorrect assignments. (Refs. 23, 37, and 38) (see Table 1).
[36] W. R. L. Lambrecht, B. Segall, W. Suttrop, M. Yoganathan, R. P. Devaty, W. J. Choyke, J. A. Edmond, J. A. Powell, and M. Alouani, Appl. Phys. Lett. **63**, 2747 (1993).
[37] M. L. Belle, N. K. Prokof'eva, and M. B. Reifman, Fiz. Tekh. Poluprovodn. **1**, 383 (1967) [Sov. Phys. Semicond. **1**, 315 (1967)].
[38] S. Logothetidis, H. M. Polatoglou, J. Petalas, D. Fuchs, and R. L. Johnson, Physica B **185**, 389 (1993).
[39] W. R. L. Lambrecht, B. Segall, M. Yoganathan, W. Suttrop, R. P. Devaty, W. J. Choyke, J. A. Edmond, J. A. Powell, and M. Alouani, Phys. Rev. B **50**, 10722 (1994).
[40] R. M. Wentzcovitch, M. Cardona, M. Cohen, and N. E. Christensen, Solid State Commun. **67**, 927 (1988).
[41] U. Rössler, Solid State Commun. **49**, 943 (1984).
[42] J. Kono, S. Takeyama, T. Takamasu, N. Miura, N. Fujimori, Y. Nishibayashi, T. Nakajima, and K. Tsuji, Phys. Rev. B **48**, 10917 (1993).
[43] C. R. Pidgeon and S. H. Groves, Phys. Rev. **186**, 824 (1958).
[44] B. Höhnerlage, U. Rössler, V. D. Phach, A. Bivas, and J. B. Grun, Phys. Rev. B **22**, 797 (1980).
[45] R. Sooryakumar, M. Cardona, and J. C. Merle, Phys. Rev. B **30**, 3261 (1984).
[46] M. P. Surh, M.-F. Li, and S. G. Louie, Phys. Rev. B **43**, 4286 (1991).
[47] F. Herman and S. Skillman, *Atomic Energy Levels* (Prentice-Hall, Englewood Cliffs, NJ, 1963).
[48] R. C. Newman and J. B. Willis, J. Phys. Chem. Solids **26**, 373 (1965).
[49] G. Davies and R. C. Newman, in *Handbook on Semiconductors*, 2nd ed., edited by S. Mahajan (North-Holland, Amsterdam, 1993), Vol. 3.
[50] J. Humlíček, K. Navrátil, M. G. Kekoua, and E. V. Khoutsishvili, Solid State Commun. **76**, 243 (1990).
[51] S. Gopalan, M. Cardona, and N. E. Christensen, Solid State Commun. **66**, 471 (1988); Phys. Rev. B **39**, 5165 (1989).